Volume 8 | Number 24 | 21 December 2021

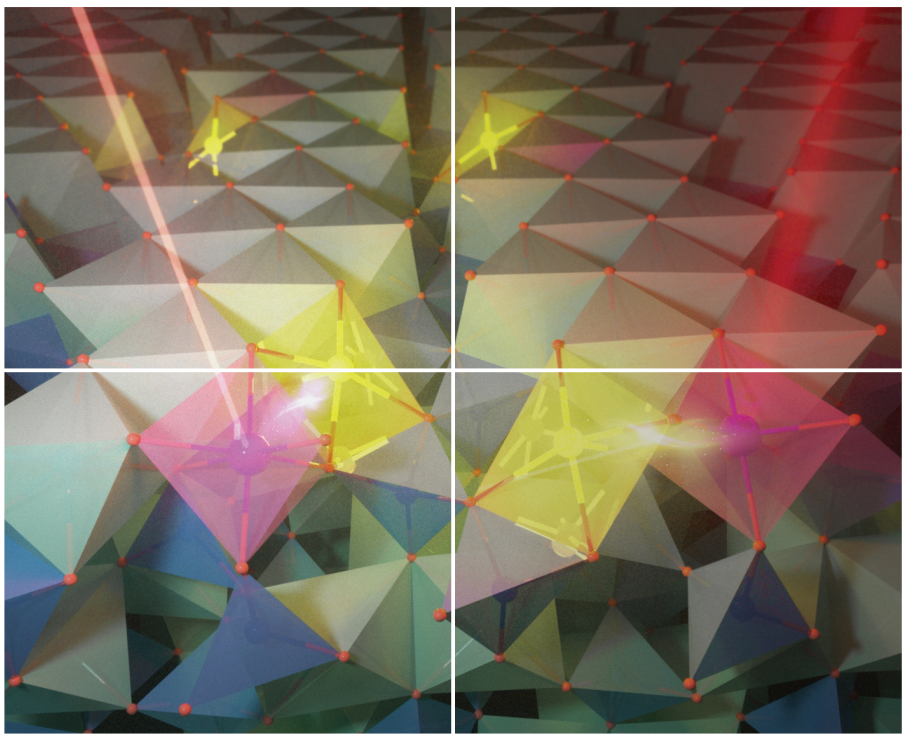

INORGANIC CHEMISTRY

FRONTIERS

CCS 中国化学会 CHINESE CHEMICAL SOCIETY

PEKING UNIVERSITY 1898

ROYAL SOCIETY OF CHEMISTRY

rsc.li/frontiers-inorganic

INORGANIC CHEMISTRY
FRONTIERS

RESEARCH ARTICLE

View Article Online
View Journal | View Issue

Check for updates

Cite this: *Inorg. Chem. Front.*, 2021, **8**, 5149

A red-light-chargeable near infrared $MgGeO_3$:Mn^{2+},Yb^{3+} persistent phosphor for bioimaging and optical information storage applications†

Weili Wang,‡[a] Shao Yan,‡[a] Yanjie Liang, *[a] Dongxun Chen, [a] Fang Wang,[b] Jingwei Liu,[a] Yi Zhang,[a] Kangning Sun[a] and Dongqi Tang*[c]

Received 13th September 2021,
Accepted 24th October 2021

DOI: 10.1039/d1qi01158h

rsc.li/frontiers-inorganic

Near-infrared (NIR) persistent phosphors have attracted extensive research interest owing to their distinct wavelength features and self-sustained luminescence properties. However, the high-energy ultraviolet light that is consistently used to charge these phosphors has compromised some promising applications, especially for biomedical imaging. Herein, we have successfully utilized long-wavelength 635 nm red-light to achieve intense NIR persistent luminescence in a $MgGeO_3$:Mn^{2+},Yb^{3+} phosphor. Seconds to minutes of 635 nm red-light charging can result in long-lasting NIR afterglow at around 680 nm for longer than 12 h. The photon trapping and detrapping processes in the $MgGeO_3$:Mn^{2+},Yb^{3+} phosphor were investigated in detail by varying the 635 nm red laser output power and the excitation duration, which indicate that a two-photon upconversion charging process is responsible for NIR persistent luminescence upon red-light illumination. The red-light-charging capability and self-sustained NIR luminescence properties make this material perfectly suited to applications across a wide number of fields, such as acting as ideal optical probes for deep-tissue bio-imaging and developing optical data storage technology for information security systems.

Published on 25 October 2021. Downloaded by Yunnan University on 8/23/2025 5:29:18 PM.

1. Introduction

Persistent luminescence materials can store excitation energy like "optical batteries" and slowly release energy as light emission when the external excitation is switched off.[1–4] In the past decades, the research and development of persistent phosphors emitting in the visible and near-infrared (NIR, 650–900 nm) spectral regions have been given substantial attention, in consideration of the increasing demands for many advanced applications ranging from night-vision surveillance to optical data storage to biomedical imaging.[5–11] In particular, for *in vivo* bioimaging, NIR persistent luminescence phosphors in the form of nanoparticles (NPs) are highly attractive imaging probes based on their inherent chemical and photophysical properties.[12] These persistent luminescence NPs, in contrast to the conventional optical probes, such as semiconductor quantum dots,[13,14] organic dyes,[15,16] and upconverting NPs,[17] not only show excellent photochemical stability and low toxicity, but also could continue emitting light for an extended time (from minutes to hours) at room temperature without the need for external irradiation.[18,19] The complete separation of photo-excitation and emission processes enable the imaging to be conducted in an excitation-free manner, and thus the optical interference (*e.g.*, tissue autofluorescence) can be completely eliminated, which will lay the foundation for high-quality bioimaging applications.[20] On top of this, the longer-wavelength red-to-NIR light that corresponds to the first biological window usually shows low light absorption and reduced light scattering in biological tissues when applied in biomedical imaging, producing a significantly improved imaging depth and a signal-to-noise ratio.[21,22]

The past decade has witnessed significant progress of NIR persistent luminescence NPs in biomedical applications, since Chermont *et al.* first introduced these NPs as imaging probes to visualize the mouse tumor.[23] Particularly in recent years, stimulated by the discovery and development of a series of Cr^{3+} doped gallate based NIR persistent phosphors with unique NIR emission and a very-long afterglow of up to hundreds of hours,[24–29] Cr^{3+} doped gallates in the form of NPs have quickly attracted significant interest and are now acting

[a]*Key Laboratory for Liquid-Solid Structure Evolution and Processing of Materials, Ministry of Education, Shandong University, Jinan 250061, China. E-mail: yanjie.liang@sdu.edu.cn*
[b]*Institute of Medical Science, the Second Hospital of Shandong University, Jinan 250033, China*
[c]*Center for Gene & Immunotherapy, the Second Hospital of Shandong University, Jinan 250033, China. E-mail: tangdq@sdu.edu.cn*
†Electronic supplementary information (ESI) available. See DOI: 10.1039/d1qi01158h
‡These authors contributed equally to this work.

Published on 25 October 2021. Downloaded by Yunnan University on 8/23/2025 5:29:18 PM.

as ideal probes for *in vivo* deep-tissue bioimaging.[30–32] However, the limited NIR afterglow time based on the consumption of stored energy and the rigorous excitation conditions (typically high-energy ultraviolet light) are the main roadblocks with regard to their application in long-term cell tracking and tumor targeting. To circumvent the limitations of the persistent luminescence-based imaging method, a photostimulated persistent luminescence (PSPL) technique has been introduced to liberate the stored energy in the deep energy traps, thus greatly prolonging the NIR afterglow time to achieve long-term tracking capability.[25,33] But the PSPL signal continues to weaken after each photostimulation cycle, due to the gradual consumption of stored energy during pre-irradiation, and the stored energy could be eventually extinguished. As a result, *in situ* charging of NIR persistent luminescence probes repeatedly with deep tissue penetrable red-to-NIR light is highly desired to address the above-mentioned issues.[34–37]

By combining the unique properties of upconversion luminescence and persistent luminescence, the upconverted persistent luminescence concept was first proposed by Liu *et al.*,[38] in which the energy traps can be successfully charged upon long-wavelength 980 nm NIR laser excitation by using the energy transfer of a "Yb^{3+}–Er^{3+}–Cr^{3+}" system. However, the persistent luminescence from Cr^{3+} after 980 nm laser charging is not strong enough, and is orders of magnitude weaker than that produced by UV light. Afterwards, the Pan group reported a two-photon upconversion charging (UCC) concept by using visible-light laser diodes for effectively charging a $LiGa_5O_8$:Cr^{3+} NIR persistent phosphor, which could emit intense persistent luminescence at the same magnitude as that produced upon high-energy UV excitation.[39] The upconversion charging strategy offers a new way to study persistent luminescence properties and develop new applications.[40,41] However, by far, the common UCC behaviors in Mn^{2+}-doped NIR persistent luminescence phosphors, including the energy absorption, upconversion kinetics, and trap charging and detrapping processes, have not been well characterized and understood, even though these Mn^{2+}-doped materials systems show significant promise in practical applications.

In this contribution, we report the detailed investigation on the UCC behaviors of an $MgGeO_3$:Mn^{2+},Yb^{3+} (hereafter referred to as MGO:Mn,Yb) NIR persistent phosphor. The generation of long-lasting NIR persistent luminescence after being charged with long-wavelength 635 nm red-light is demonstrated. The trapping and detrapping processes with a 635 nm red laser as the excitation source have been comprehensively studied by spectroscopic characterization and thermoluminescence measurements, suggesting that the MGO:Mn,Yb phosphor holds great potential for bioimaging and optical information storage applications.

2. Experimental section

2.1. Sample preparation

The MGO:Mn,Yb phosphors were fabricated using a high-temperature solid-state reaction technique. Stoichiometric amounts of MgO (99.99%, Aladdin), GeO_2 (99.99%, Aladdin), MnO (99.99%, Aladdin), and Yb_2O_3 (99.99%, Aladdin) powders were thoroughly mixed and ground in an agate mortar. The mixed powder was then pressed into performed discs with a diameter of ~11 mm using a dry pressing machine. After that, the discs were fired at 1250 °C in air for 2 h to obtain the final samples. For the phosphor film, the synthesized phosphor powders were homogeneously mixed with the silicone elastomer in a weight ratio of 1 : 1 to form the phosphor slurries. Then the slurries were molded on a thin copper sheet. Baffle plates were used to control the size and thickness of the phosphor slurries. The phosphor films were obtained after heating at 80 °C for 0.5 h and 120 °C for 2 h in an oven.

2.2. Characterization

The crystal structures of the as-synthesized MGO:Mn,Yb phosphors were characterized on a DMAX-2500PC powder X-ray diffractometer with Cu $K\alpha_1$ radiation (λ = 1.5406 Å). The Rietveld refinement was achieved using general structure analysis system (GSAS) software. The spectral properties of the phosphors, including photoluminescence emission and excitation spectra, persistent luminescence decay curves, and persistent luminescence excitation and emission spectra, were analyzed using an Edinburgh FLS1000 spectrofluorometer which was equipped with a 450 W xenon arc lamp and a photomultiplier tube (measurement range, 200–900 nm). A 500 mW 635 nm laser diode was used to excite the samples. All spectra were corrected for the optical system responses. The fluorescence decay curves were obtained from the same fluorescence spectrophotometer with a μF900 flash lamp as the excitation source. The thermoluminescence spectra were recorded using an SL08 thermoluminescence setup (Guangzhou Rongfan Science and Technology Co., Ltd; heating rate, 4 °C s^{-1}). Before all the spectral measurements, the samples were heat-treated in a furnace at 400 °C to completely empty the energy traps in the material. The 635 nm red laser was used as the excitation source in all of the imaging experiments. Several conditions were evaluated for the *in vitro* experiments. NIR persistent luminescence images of a pre-irradiated MGO:Mn,Yb sample are recorded using an IVIS imaging system after being covered with a 1 cm pork slice. The sample was pre-excited with the 100 mW 635 red laser for 1 min. The exposure time of the imaging system is 5 s. The *in situ* red-light charging and imaging experiments were performed by covering the MGO:Mn,Yb phosphor powders with a ~0.5 cm thickness pork slice. The exposure time of the imaging system is set to be 15 s. A commercial micro-laser engraving machine loaded with the 635 nm red laser (maximum output: 1.20 W) was used to demonstrate the application of optical information storage on the prepared phosphor discs and phosphor films. The laser engraving machine was driven by a computer program and worked in a bit-by-bit mode. The phosphor discs and phosphor films after data recording were heated up to 200 °C for the encoded pattern readout. The write-in and read-out processes were recorded using a Canon EOS 800D digital camera.

 This journal is © the Partner Organisations 2021

Published on 25 October 2021. Downloaded by Yunnan University on 8/23/2025 5:29:18 PM.

3. Results and discussion

3.1. Crystal structure and phase purity of MGO:Mn,Yb phosphors

The XRD patterns of the as-synthesized MGO:Mn,Yb phosphors are shown in Fig. 1a. All XRD peaks are in line with the standard card of $MgGeO_3$ crystals (JCPDS No. 76-1387). The co-doping of Mn^{2+} and Yb^{3+} ions has no obvious influence on the crystal structure of the $MgGeO_3$ host, indicating the successful synthesis of MGO:Mn,Yb phosphors. The $MgGeO_3$ compound crystallizes in the orthorhombic system with a space group of *Pbca* (61), which is composed 6-fold coordinated Mg^{2+} and 4-fold coordinated Ge^{4+}, forming [MgO_6] octahedra and [GeO_4] tetrahedra, respectively, as shown in Fig. 1b. In this structure, the Mn^{2+} emitters (r = 0.072 nm, CN = 6) prefer to substitute for the octahedral sites of Mg^{2+} ions (r = 0.067 nm, CN = 6) in the host lattice, considering their similar ionic radii and same valence states, while the Yb^{3+} ions most probably occupy the sites of Mg^{2+} ions in the host structure.

Rietveld XRD refinement was performed to further understand the crystal structure and extract the lattice parameters of the as-synthesized MGO:Mn,Yb phosphors. The experimental XRD data, the corresponding Rietveld refinement results, the Bragg reflections and the profile difference between the experimental and calculated values are shown in Fig. 1c. It is found that the observed and calculated XRD patterns coincide well with each other. The refinement results converge well and yield an *R*wp value of 8.61% and an R_p value of 6.12%, indicating the formation of a single phase with no evidence of an impurity phase. The calculated lattice parameters of MGO:Mn, Yb are presented in Table S1 in the ESI.†

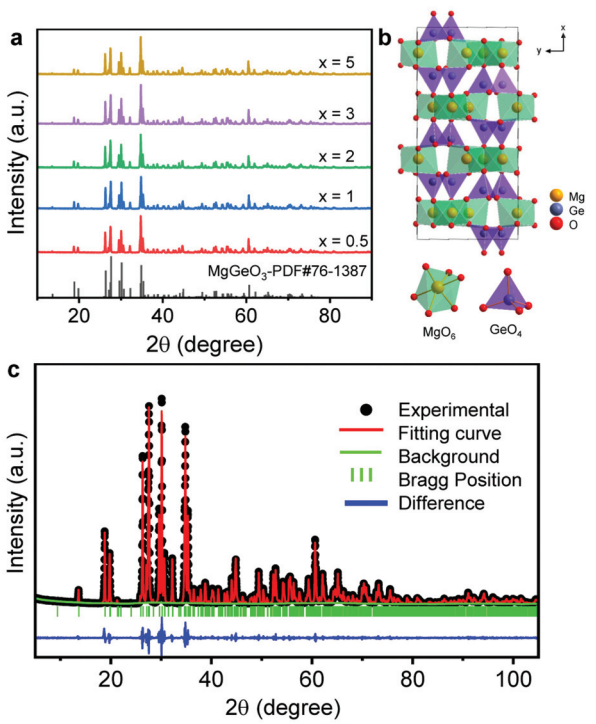

Fig. 1 (a) XRD patterns of $MgGeO_3$:x%Mn^{2+},0.1%Yb^{3+} (x = 0.5, 1, 2, 3 and 5) phosphors. (b) Schematic diagram of the crystal structure of $MgGeO_3$. (c) Rietveld refinement of the MGO:Mn,Yb phosphor.

3.2. Photoluminescence properties of the MGO:Mn,Yb phosphor

The photoluminescence emission and excitation spectra of the MGO:Mn,Yb phosphor at room temperature are shown in Fig. 2a. When exciting with 295 nm light, the MGO:Mn,Yb phosphor exhibits a broadband emission band covering a wavelength range over 600–800 nm with an emission peak at 680 nm. The intense NIR emission is the characteristic of Mn^{2+} ions that are located in an octahedral environment in the host compound and can be attributed to the $^4T_1 \rightarrow {}^6A_1$ transition of Mn^{2+}.[42,43] The photoluminescence excitation spectrum monitored at 680 nm contains several bands in the UV and visible spectral regions. The broad absorption band peaking at 295 nm can be assigned to the charge transfer transition of Mn^{2+}.[44] The weak excitation peaks in a wavelength range of 340–460 nm can be attributed to the typical electron transitions of Mn^{2+} from the $^6A_1$ ground state to the $^4T_1$(P), ^4E(D), $^4T_2(^4D)$, $^4A_1(^4G)/^4E(^4G)$ and $^4T_2$(G) excited states, respectively.[45,46] The decay time measurement of the Mn^{2+} emission in the MGO:Mn,Yb phosphor under 295 nm excitation at room temperature is shown in Fig. 2b. The decay curve follows single exponential kinetics perfectly and the decay time of the Mn^{2+} emission is determined to be 10.71 ms, which is consistent with those of other typical Mn^{2+}-activated phosphors.[47–49]

3.3. Red-light-activated NIR persistent luminescence properties

Besides intense NIR photoluminescence, the excitation with high-energy UV light can effectively charge the $MgGeO_3$:Mn^{2+} phosphor and result in long-lasting NIR afterglow, as reported in previous research.[50–52] However, in comparison with the most common high-energy UV lamp used for achieving NIR afterglow, it is demonstrated here that long-wavelength

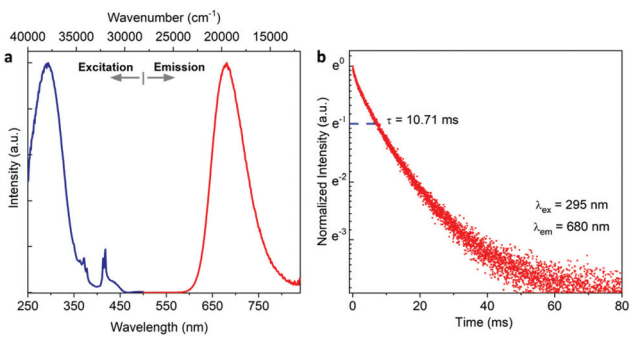

Fig. 2 (a) Photoluminescence emission and excitation spectra of the MGO:Mn,Yb phosphor. The emission spectrum is acquired upon 295 nm excitation and the excitation spectrum is obtained by monitoring at 680 nm emission. (b) Fluorescence lifetime decay of the MGO:Mn,Yb phosphor under 295 nm light excitation.

Published on 25 October 2021. Downloaded by Yunnan University on 8/23/2025 5:29:18 PM.

635 nm red-light can also induce exceptional NIR persistent luminescence in the MGO:Mn,Yb phosphor. Moreover, the NIR persistent luminescence performances are strongly dependent on the concentrations of Mn^{2+} emitters and Yb^{3+} co-dopants. The optimum persistent luminescence performance is achieved in the MGO:1%Mn,0.1%Yb phosphor, as shown in ESI Fig. S1.† Fig. 3a shows the NIR persistent luminescence decay curve of the MGO:Mn,Yb phosphor after being charged with the 635 nm red laser for 15 min. The afterglow duration was recorded as 12 h, which is comparable to that produced by the standard 254 nm UV lamp. As can be seen in Fig. 3a, the afterglow intensity is still considerably high after 12 h decay, indicating that persistent NIR light emission after red-light charging could last much longer than 12 h. The persistent luminescence decay curve was also plotted as a function of the NIR afterglow intensity (I) *versus* decay time (t) in a double-logarithmic coordinate system, as shown in ESI Fig. S2.† The slope of the decay curve is determined to be 1.49, indicating that the tunneling mechanism occurs during the persistent luminescence process.[53,54] The upper inset of Fig. 3a shows a persistent luminescence emission spectrum acquired at 1 h after stopping excitation, which shows the characteristic broadband emission of Mn^{2+} and an identical profile to the photoluminescence emission spectrum, indicating that the NIR afterglow originates from the Mn^{2+} emitting center.

The long-lasting NIR persistent luminescence of MGO:Mn,Yb after red-light charging was also visually evaluated by imaging experiments, as shown in Fig. 3b. After exposure to the 635 nm red laser for 15 min, the NIR persistent luminescence signal can be seen with the naked eye for only 10 min, because the NIR persistent emission peaking at 680 nm from the material is less efficiently sensed by the human eye in a dark environment. However, with the help of a night-vision monocular, the changes of NIR emission brightness with a decay time up to 12 h could be clearly observed. The decay time-dependent persistent luminescence images clearly show that the MGO:Mn,Yb phosphor can be effectively charged by the long-wavelength 635 nm red-light, inducing a remarkable NIR afterglow for more than 12 h.

To further understand the charging process upon 635 nm red-light illumination in the MGO:Mn,Yb phosphor, we studied the relationship between the NIR afterglow intensity and the output power of the 635 nm red laser. In our experiment, we excited the MGO:Mn,Yb phosphor using the 635 nm red laser with the output powers ranging from 5 mW to 100 mW. The phosphor was irradiated for 1 min at each fixed power and the NIR afterglow decay curves monitoring at 680 nm were recorded after each excitation, as shown in Fig. 4a. The persistent luminescence intensity at a decay time of 30 s in each decay curve was selected as the reference point to obtain the plot of persistent luminescence intensity (I_{30s}) *versus* the excitation power of the 635 nm laser (P), as shown by the ln(I)–ln(P) coordinates in Fig. 4b. As shown in Fig. 4, the NIR afterglow intensity increases as the excitation power increases. It is found that the dependence of the afterglow intensity and output power can be expressed by the formula I–$P^{1.35}$ as the excitation power changes in the range of 5–100 mW, which is in accordance with the characteristic of the upconversion process.[55] Such a quadratic relationship indicates the occurrence of an upconversion charging process, in which two 635 nm red photons are absorbed to pump the Mn^{2+} to the delocalization state and then fill the energy traps (generally lattice defects or impurities[56]), as presented in the energy level diagram in Fig. 4b. The absorption band of Mn^{2+} in the red part (550–650 nm) of the excitation spectrum paves the way for the successful absorption of a low energy 635 nm

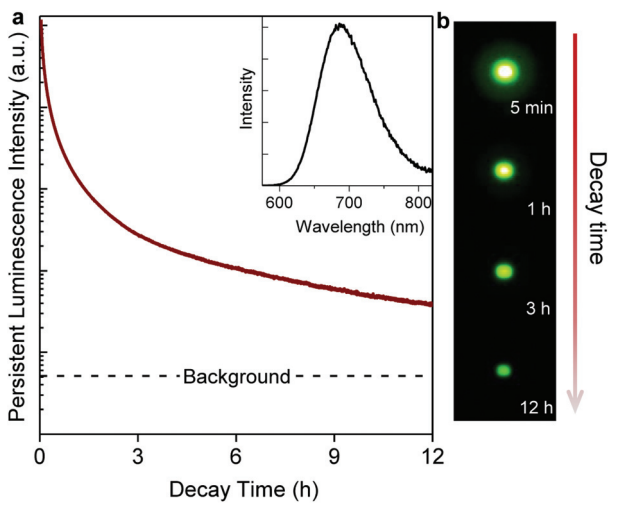

Fig. 3 (a) NIR persistent luminescence of the MGO:Mn,Yb phosphor at room temperature. NIR persistent luminescence decay curve monitored at 680 nm after irradiation with the 635 nm red laser for 10 min (output power, 500 mW). The inset shows the NIR persistent luminescence emission spectrum recorded at 1 h after stopping irradiation. (b) NIR persistent luminescence images of the MGO:Mn,Yb phosphor taken at different decay times (5 min to 12 h). The images were taken using a digital camera that was connected to a night vision monocular. The imaging parameters are manual/ISO 400/1 s (5 min) and manual/ISO 400/10 s (1 h, 3 h and 12 h), respectively.

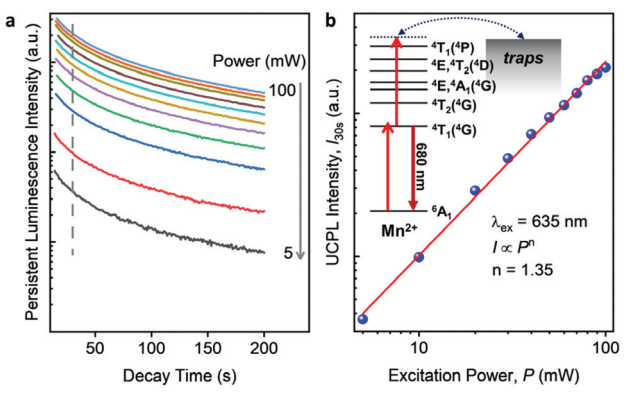

Fig. 4 (a) NIR persistent luminescence decay curves of the MGO:Mn,Yb phosphor irradiated with the 635 nm red laser with different output powers (5–100 mW) for 1 min. (b) Double-logarithmic plot of NIR persistent luminescence intensities at 30 s (I_{30s}) *versus* the laser powers (P).

This journal is © the Partner Organisations 2021

Published on 25 October 2021. Downloaded by Yunnan University on 8/23/2025 5:29:18 PM.

photon due to the $^6A_1 \rightarrow {}^4T_1$ transition of Mn^{2+} emitters, as shown in ESI Fig. S3.† Meanwhile, the long stable-state luminescence lifetime of the $^4T_1$ energy level of Mn^{2+} can act as a metastable state (Fig. 2b), and a second 635 nm red photon further pumps the Mn^{2+} to the high-energy delocalized state, owing to the excited-state absorption phenomenon, as observed in in a $LiGa_5O_{12}:Cr^{3+}$ phosphor.[39] The delocalized electrons could be captured by and stored in the energy traps below the bottom of the conduction band, thus enabling the occurrence of intense NIR persistent luminescence in the MGO:Mn,Yb phosphor due to thermal or other physical stimulations.

3.4. Thermoluminescence properties of the MGO:Mn,Yb phosphor

The above experimental results have revealed that 635 nm red laser excitation can generate intense NIR persistent luminescence in the MGO:Mn,Yb phosphor *via* the upconversion charging process. To gain further insight into the trap properties and the interactions between the Mn^{2+} emitters and the traps in this phosphor, we conducted thermoluminescence measurements under the excitation of a tunable 635 nm laser (output power, 5–400 mW), which can provide information related to the trap density and trap distribution in the phosphor. Two excitation conditions were systematically tuned when measuring the TL curves: varying the laser output power between 5 mW and 400 mW with a fixed excitation duration of 60 s and varying the excitation duration between 10 s and 900 s with a fixed output power of 40 mW and 400 mW, respectively. Fig. 5a shows the TL spectra of the MGO:Mn,Yb phosphor after illumination with the 635 nm red laser with different output powers. The obtained TL curves in Fig. 5a show varied TL intensities but almost identical spectral shapes. Each TL curve exhibits two broad bands peaking at ~365 K (peak 1, low temperature band) and ~430 K (peak 2, high temperature band), respectively, suggesting that two kinds of traps, shallow traps and deep traps, exist in the MGO:Mn,Yb phosphor. To figure out the details of these traps, the TL curves of MGO:Mn and MGO:Mn,Yb phosphors were recorded after 635 nm laser excitation, as shown in ESI Fig. S4.† After co-doping Yb^{3+} ions, the integrated TL intensity is greatly enhanced along with the appearance of an additional TL band at 365 K, which is in good agreement with a previous study.[57] Therefore, the shallow traps in the MGO:Mn,Yb phosphor can be attributed to the Yb^{3+} co-doping, while the deep trap located at 430 K is probably related to the intrinsic defects of the host (*e.g.*, oxygen vacancies). It is also noted that the TL spectrum after 635 nm red-light illumination is almost consistent with that after irradiation with the 254 nm UV lamp (ESI Fig. S5†). However, a small peak shift to higher temperature and an obvious increase in deep trap intensity are observed, indicating that the 635 nm red laser cannot depopulate the deep-trapped electrons while the 254 nm UV lamp can. As the output power increases from 5 mW to 400 mW, the TL intensity shows a rapid increase, while the positions of two band maxima are independent of the laser power. By fitting the integrated TL intensity *versus* excitation power in the log–log plot (upper inset of Fig. 5a), the *I*–*P* curve is in good agreement with a quadratic relationship (I–$P^{1.27}$) when the excitation power increases over 5–100 mW, further indicating that the two-photon upconversion excitation process is involved in the NIR persistent luminescence process upon red-light excitation. The upper inset in Fig. 5a also shows that the slope of the fitting line starts to decrease as the excitation power further increases in the range of 100–400 mW, which is probably due to the photostimulated detrapping process during red-light charging.[39,41]

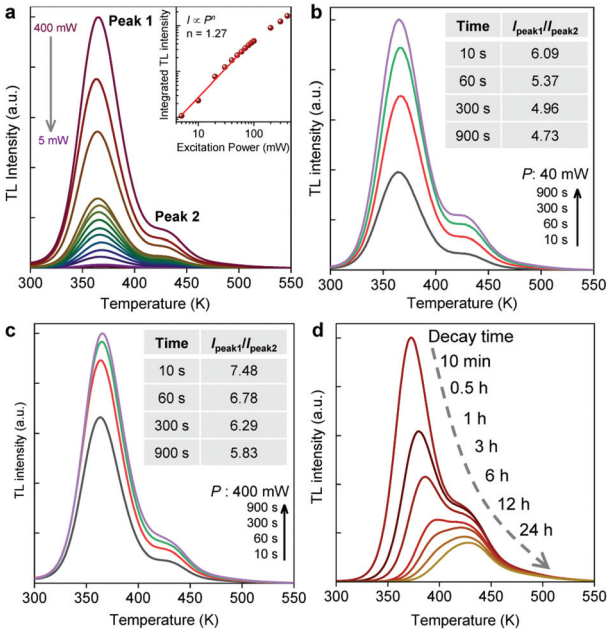

Fig. 5 (a) TL spectra monitored at 680 nm over 300–550 K after irradiation with the 635 nm red laser with different output powers (5–400 mW). The exposure time is 60 s for each measurement. The TL curves are recorded at 60 s after excitation. (b) TL spectra after excitation with the 40 mW red laser for different durations from 10 s to 900 s. Each spectrum is recorded at 60 s after excitation. (c) TL spectra after excitation with the 400 mW red laser for different durations from 10 s to 900 s. (d) TL curves monitored at 680 nm emission over 300–550 K for samples with different decay times from 10 min to 24 h.

We further measured the TL spectra of the MGO:Mn,Yb phosphor after illumination with a fixed output power (40 mW and 400 mW, respectively), but with different durations from 10 s to 900 s. As shown in Fig. 5b, after illuminating the sample with the 40 mW 635 nm red laser, the intensities of the low temperature band and high temperature band kept increasing, while the positions of the TL band maxima remained almost constant with the increase of exposure time from 10 s to 900 s. However, it is found that the TL intensity ratio of the low-temperature band and high-temperature band decreases monotonically from 6.09 to 4.73 as the excitation duration increases, indicating that these two kinds of traps have divergent increase trends and the intensity of deep traps increases faster than that of shallow traps. When the output

Published on 25 October 2021. Downloaded by Yunnan University on 8/23/2025 5:29:18 PM.

power of the red laser is fixed at 500 mW, as shown in Fig. 5c, the increase of low temperature band intensity still does not keep pace with that of the high temperature band. The TL intensity ratio decreases from 7.48 to 5.83 with increasing excitation duration, while the value at a fixed irradiation time is always higher than that at 40 mW (Fig. 5b) due to the higher excitation intensity. The divergent increase trend of shallow traps and deep traps is probably due to different stimulation effects of the 635 nm red laser.[38] Under excitation with the 635 nm red laser, the shallow traps and deep traps in the material are filled through the two-photon upconversion charging process. Meanwhile, the long-wavelength 635 nm red-light can also promote the trapped electrons in the shallow traps to the delocalized conduction band *via* a photostimulation process, which will cause the depopulation of electrons in the shallow traps, while it is not very effective at delocalizing the electrons in the deep traps. Thus, with the increase of the excitation duration, the population in the deep traps increases more rapidly than that in the shallow traps.

Decay time-dependent TL measurements by monitoring 680 nm emission were also recorded, and the TL curves are shown in Fig. 5d. It is found that the intensity of shallow traps at low-temperature decreases steeply, which is barely recognizable after 12 h of natural decay. On the other hand, the intensity of deep traps at high temperature decreases gradually as the decay time increases, while the position of the peak maximum almost remains unchanged with the increase of decay time. After 24 h natural decay, the intensity of deep traps also drops markedly because these deep-trapped electrons are released at a very slow rate for long-lasting NIR afterglow of the MGO:Mn,Yb phosphor.

3.5. Bioimaging and optical information storage applications

The developed MGO:Mn,Yb phosphor exhibits a unique red-light chargeable capability and self-sustained NIR luminescence, which enable it to have high promise for bioimaging and optical information storage applications. For the MGO:Mn,Yb sample pre-irradiated with the 635 nm red laser (100 mW, 1 min), the NIR persistent luminescence signals from the sample (50 mg) could be clearly detected using the IVIS imaging system for more than 30 min when it was covered with the 1 cm pork slice, which further indicates that the MGO:Mn,Yb phosphor can be effectively charged with 635 nm red-light. The afterglow intensity decreases gradually with prolonging decay time and the imaging signals become undetectable for about 60 min, as shown in Fig. 6a. Repeated *in situ* charging through the pork tissue (0.5 cm) with 635 nm red-light was further tested. The imaging results are presented in Fig. 6b–e. It is found that the 635 nm red laser can effectively charge the MGO:Mn,Yb phosphor *in situ* because of its good tissue penetration capability. The MGO:Mn,Yb sample can still provide high-quality and clear images within 30 min after *in situ* excitation. More importantly, NIR persistent luminescence signals from the sample have good reproducibility after repeatedly charging with the 635 nm red laser, as shown in Fig. 6c–e. In the 2nd, 3rd and 4th imaging cycles, the

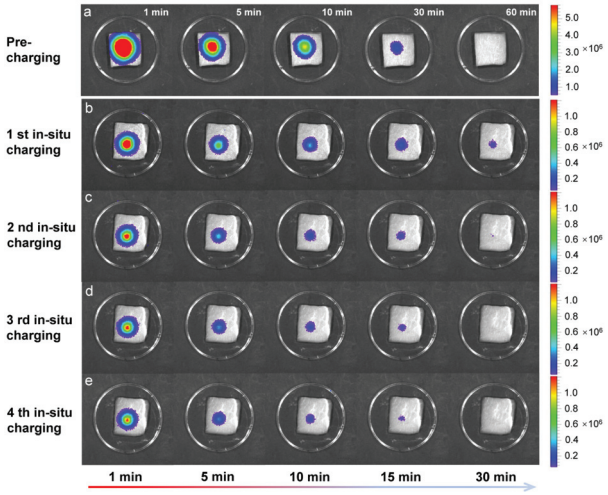

Fig. 6 Deep tissue *in vitro* imaging application by using the MGO:Mn,Yb sample. (a) NIR persistent luminescence images of the pre-irradiated MGO:Mn,Yb sample (50 mg) when covered with the 1 cm pork slice. The sample was pre-excited with the 100 mW 635 red laser for 1 min. The exposure time of the imaging system is 5 s. (b–e) Repeated *in vitro* imaging after *in situ* excitation of the MGO:Mn,Yb sample (50 mg) covered with the 0.5 cm pork slice using the 635 nm red laser (100 mW, 1 min). The time interval for repeated imaging is set to be 30 min. The exposure time of the imaging system is 15 s.

MGO:Mn,Yb phosphor can be recharged *in situ* and it continuously emits NIR light for a desired time (30 min) to provide a clear NIR afterglow imaging signal, suggesting the reliable stability and repeatability of this material for deep-tissue *in vivo* bioimaging. Furthermore, NIR persistent luminescence imaging can also be realized by directly charging with long-wavelength red-light when the MGO:Mn,Yb sample is covered with the 1 cm thickness pork slice, as shown in ESI Fig. S6.†

A series of optical data recording and read-out experiments were also carried out on MGO:Mn,Yb phosphor discs and flexible phosphor films. A commercial micro-laser engraving machine loaded with a 635 nm red laser is used to write in specific patterns *via* a bit-by-bit mode, as shown in Fig. 7a. After data recording, the encoded information on phosphor discs and phosphor films are invisible in a bright indoor environment because the NIR afterglow signal is submerged by the overwhelming indoor light (Fig. 7b and c). Meanwhile, these input records cannot be recognized with the naked eye in the dark after a certain decay time (tens of seconds) owing to the low sensitivity of the naked eye to the red-to-NIR afterglow emission. However, these encoded patterns can be observed clearly with human eyes when the phosphor discs and phosphor films are heated to a higher temperature due to the massive release of stored excitation energy as red-to-NIR light emission. Fig. 7d and e show the photographs of decoded patterns in red-to-NIR emission on different phosphor discs when heated to 200 °C after 1 h natural decay. The input stick figures of a person when studying, smiling, playing and thinking (Fig. 7d) and Chinese characters of Shandong

 This journal is © the Partner Organisations 2021

Published on 25 October 2021. Downloaded by Yunnan University on 8/23/2025 5:29:18 PM.

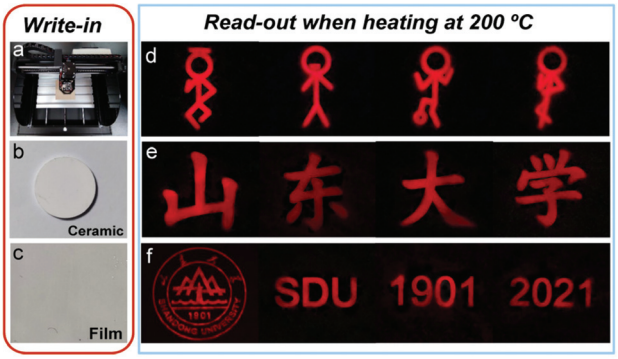

Fig. 7 Application of the MGO:Mn,Yb persistent phosphor for optical information storage. (a) Photograph of a commercialized micro-laser engraving machine. (b and c) Phosphor disc and phosphor film of MGO:Mn,Yb after data recording with a computer program controlled 635 nm red laser under an indoor-lighting environment. (d and e) Optical read-out of stick figures and Chinese characters on the phosphor discs after heating at 200 °C in the dark. (f) Luminescence pattern read-out from the flexible phosphor film when heating at 200 °C in the dark.

University (Fig. 7e) on different phosphor discs become visible in the dark when heated at high temperature. Moreover, the luminescence patterns of the Shandong University logo, SDU letters (abbreviation of Shandong University) and Arabic numbers (1901 and 2021) were also written in the phosphor film by using the 635 nm red laser, and were invisible in bright and dark environments. After heating at 200 °C, bright luminescence images depicting the recorded information clearly appear in the dark. This unique red-light write-in and temperature-stimulated read-out mode provide great opportunities for Mn^{2+}-doped NIR storage phosphors in the field of repeatedly erasable information security systems.

4. Conclusion

In conclusion, we have investigated a two-photon upconversion charging process in MGO:Mn,Yb phosphors by using long-wavelength 635 nm red laser excitation. The MGO:Mn,Yb phosphor exhibits single band NIR persistent luminescence peaking at around 680 nm with a long afterglow time of more than 12 h after 635 nm red-light illumination. A quadratic relationship between the persistent luminescence intensity and excitation power reveals that the sequential absorption of two 635 nm red photons can promote the Mn^{2+}-doped material system from the ground state to the high-energy delocalized state *via* an upconversion charging process. The two-photon upconversion charging technique in these Mn^{2+}-activated NIR persistent phosphors enables the *in situ* charging of persistent optical probes *via* a tissue-friendly red-light source to achieve long-term tracking capability in biomedical imaging. Moreover, the unique write-in (by red laser) and read-out (by thermal stimulation) modes also hold great promise for information security applications.

Conflicts of interest

There are no conflicts to declare.

Acknowledgements

This work was supported by the financial support from the National Natural Science Foundation of China (grant no. 51902184), Natural Science Foundation of Shandong Province (grant no. ZR2019BEM028) and the "Qi-Lu Young Scholar Fund" (grant no. 31370088963167) from Shandong University.

References

1 J. Hölsä, Persistent luminescence beats the afterglow: 400 years of persistent luminescence, *Electrochem. Soc. Interface*, 2009, **18**, 42–45.
2 K. Van den Eeckhout, P. F. Smet and D. Poelman, Persistent Luminescence in Eu^{2+}-Doped Compounds: A Review, *Materials*, 2010, **3**, 2536–2566.
3 J. Xu and S. Tanabe, Persistent luminescence instead of phosphorescence: history, mechanism, and perspective, *J. Lumin.*, 2019, **205**, 581–620.
4 D. Poelman, D. Van der Heggen, J. Du, E. Cosaert and P. F. Smet, Persistent phosphors for the future: fit for the right application, *J. Appl. Phys.*, 2020, **128**, 240903.
5 S. Sun, H. Wang and X. Yan, Engineering persistent luminescence nanoparticles for biological applications: from biosensing/bioimaging to theranostics, *Acc. Chem. Res.*, 2018, **51**, 1131–1143.
6 Y. Li, M. Gecevicius and J. Qiu, Long persistent phosphors-from fundamentals to applications, *Chem. Soc. Rev.*, 2016, **45**, 2090–2136.
7 Z. Zhou, Y. Li and M. Peng, Near-infrared persistent phosphors: synthesis, design, and applications, *Chem. Eng. J.*, 2020, **399**, 125688.
8 Y. Zhuang, L. Wang, Y. Lv, T. Zhou and R. Xie, Optical data storage and multicolor emission readout on flexible films using deep-trap persistent luminescence materials, *Adv. Funct. Mater.*, 2017, **28**, 1705769.
9 J. Xu, D. Murata, J. Ueda, B. Viana and S. Tanabe, Toward rechargeable persistent luminescence for the first and third biological windows via persistent energy transfer and electron trap redistribution, *Inorg. Chem.*, 2018, **57**, 5194–5203.
10 L. Yuan, Y. Jin, Y. Su, H. Wu, Y. Hu and S. Yang, Optically stimulated luminescence phosphors: principles, applications, and prospects, *Laser Photonics Rev.*, 2020, **14**, 2000123.
11 J. Ueda, S. Miyano and S. Tanabe, Formation of deep electron traps by Yb^{3+} codoping leads to super-long persistent luminescence in Ce^{3+}-doped yttrium aluminum gallium garnet phosphors, *ACS Appl. Mater. Interfaces*, 2018, **10**, 20652–20660.

Published on 25 October 2021. Downloaded by Yunnan University on 8/23/2025 5:29:18 PM.

12 T. Maldiney, A. Bessière, J. Seguin, E. Teston, S. K. Sharma, B. Viana, A. J. J. Bos, P. Dorenbos, M. Bessodes, D. Gourier, D. Scherman and C. Richard, The in vivo activation of persistent nanophosphors for optical imaging of vascularization, tumours and grafted cells, *Nat. Mater.*, 2014, **13**, 418–426.

13 B. A. Kairdolf, A. M. Smith, T. H. Stokes, M. D. Wang, A. N. Young and S. Nie, Semiconductor quantum dots for bioimaging and biodiagnostic applications, *Annu. Rev. Anal. Chem.*, 2013, **6**, 143–162.

14 O. T. Bruns, T. S. Bischof, D. K. Harris, D. Franke, Y. Shi, L. Riedemann, A. Bartelt, F. B. Jaworski, J. A. Carr, C. J. Rowlands, M. W. B. Wilson, O. Chen, H. Wei, G. W. Hwang, D. M. Montana, I. Coropceanu, O. B. Achorn, J. Kloepper, J. Heeren, P. T. C. So, D. Fukumura, K. F. Jensen, R. K. Jain and M. G. Bawendi, Next-generation in vivo optical imaging with short-wave infrared quantum dots, *Nat. Biomed. Eng.*, 2017, **1**, 0056.

15 S. Luo, E. Zhang, Y. Su, T. Cheng and C. Shi, A review of NIR dyes in cancer targeting and imaging, *Biomaterials*, 2011, **32**, 7127–7138.

16 S. Zhu, R. Tian, A. L. Antaris, X. Chen and H. Dai, Near-infrared-II molecular dyes for cancer imaging and surgery, *Adv. Mater.*, 2019, **31**, 1900321.

17 J. Zhou, Q. Liu, W. Feng, Y. Sun and F. Li, Upconversion luminescent materials: advances and applications, *Chem. Rev.*, 2015, **115**, 395–465.

18 J. Wang, Q. Ma, Y. Wang, H. Shen and Q. Yuan, Recent progress in biomedical applications of persistent luminescence nanoparticles, *Nanoscale*, 2017, **9**, 6204–6218.

19 T. Ai, W. Shang, H. Yan, C. Zeng, K. Wang, Y. Gao, T. Guan, C. Fang and J. Tian, Near infrared-emitting persistent luminescent nanoparticles for Hepatocellular Carcinoma imaging and luminescence-guided surgery, *Biomaterials*, 2018, **167**, 216–225.

20 T. Lecuyer, E. Teston, G. Ramirez-Garcia, T. Maldiney, B. Viana, J. Seguin, N. Mignet, D. Scherman and C. Richard, Chemically engineered persistent luminescence nanoprobes for bioimaging, *Theranostics*, 2016, **6**, 2488–2524.

21 A. M. Smith, M. C. Mancini and S. Nie, Bioimaging: second window for in vivo imaging, *Nat. Nanotechnol.*, 2009, **4**, 710–711.

22 G. Hong, A. L. Antaris and H. Dai, Near-infrared fluorophores for biomedical imaging, *Nat. Biomed. Eng.*, 2017, **1**, 0010.

23 Q. L. M. de Chermont, C. Chaneac, J. Seguin, F. Pelle, S. Maitrejean, J. P. Jolivet, D. Gourier, M. Bessodes and D. Scherman, Nanoprobes with near-infrared persistent luminescence for in vivo imaging, *Proc. Natl. Acad. Sci. U. S. A.*, 2007, **104**, 9266–9271.

24 Z. Pan, Y. Lu and F. Liu, Sunlight-activated long-persistent luminescence in the near-infrared from Cr^{3+}-doped zinc gallogermanates, *Nat. Mater.*, 2011, **11**, 58–63.

25 F. Liu, W. Yan, Y. Chuang, Z. Zhen, J. Xie and Z. Pan, Photostimulated near-infrared persistent luminescence as a new optical read-out from Cr^{3+}-doped $LiGa_5O_8$, *Sci. Rep.*, 2013, **3**, 1554.

26 M. Allix, S. Chenu, E. Véron, T. Poumeyrol, E. A. Kouadri-Boudjelthia, S. Alahraché, F. Porcher, D. Massiot and F. Fayon, Considerable improvement of long-persistent luminescence in germanium and tin substituted $ZnGa_2O_4$, *Chem. Mater.*, 2013, **25**, 1600–1606.

27 Y. Li, S. Zhou, Y. Li, K. Sharafudeen, Z. Ma, G. Dong, M. Peng and J. Qiu, Long persistent and photo-stimulated luminescence in Cr^{3+}-doped Zn-Ga-Sn-O phosphors for deep and reproducible tissue imaging, *J. Mater. Chem. C*, 2014, **2**, 2657–2663.

28 J. Xu, J. Ueda and S. Tanabe, Toward tunable and bright deep-red persistent luminescence of Cr^{3+} in garnets, *J. Am. Ceram. Soc.*, 2017, **100**, 4033–4044.

29 X. Zhou, W. Geng, J. Li, Y. Wang, J. Ding and Y. Wang, An ultraviolet-visible and near-infrared-responded broadband NIR phosphor and its NIR spectroscopy application, *Adv. Opt. Mater.*, 2020, **8**, 1902003.

30 A. Abdukayum, J. Chen, Q. Zhao and X. Yan, Functional near infrared-emitting Cr^{3+}/Pr^{3+} co-doped zinc gallogermanate persistent luminescent nanoparticles with superlong afterglow for in vivo targeted bioimaging, *J. Am. Chem. Soc.*, 2013, **135**, 14125–14133.

31 Z. Li, Y. Zhang, X. Wu, L. Huang, D. Li, W. Fan and G. Han, Direct aqueous-phase synthesis of sub-10 nm "luminous pearls" with enhanced in vivo renewable near-infrared persistent luminescence, *J. Am. Chem. Soc.*, 2015, **137**, 5304–5307.

32 L. Liang, N. Chen, Y. Jia, Q. Ma, J. Wang, Q. Yuan and W. Tan, Recent progress in engineering near-infrared persistent luminescence nanoprobes for time-resolved biosensing/bioimaging, *Nano Res.*, 2019, **12**, 1279–1292.

33 Y. J. Chuang, Z. Zhen, F. Zhang, F. Liu, J. P. Mishra, W. Tang, H. Chen, X. Huang, L. Wang, X. Chen, J. Xie and Z. Pan, Photostimulable near-infrared persistent luminescent nanoprobes for ultrasensitive and longitudinal deep-tissue bio-imaging, *Theranostics*, 2014, **4**, 1112–1122.

34 J. Ueda, J. L. Leaño, C. Richard, K. Asami, S. Tanabe and R. Liu, Broadband near-infrared persistent luminescence of $Ba[Mg_2Al_2N_4]$ with Eu^{2+} and Tm^{3+} after red light charging, *J. Mater. Chem. C*, 2019, **7**, 1705–1712.

35 L. Huang, L. Lin, W. Xie, Z. Qiu, H. Ni, H. Liang, Q. Tang, L. Cao, J. Meng and F. Li, Near-infrared persistent luminescence in a Cr^{3+}-doped perovskite for low-irradiance imaging, *Chem. Mater.*, 2020, **32**, 5579–5588.

36 J. Du and D. Poelman, Red-light-activated red-emitting persistent luminescence for multicycle bioimaging: a case study of $CaS:Eu^{2+},Dy^{3+}$, *J. Phys. Chem. C*, 2020, **124**, 16586–16595.

37 X. Chen, Y. Li, K. Huang, L. Huang, X. Tian, H. Dong, R. Kang, Y. Hu, J. Nie, J. Qiu and G. Han, Trap energy upconversion-like near-infrared to near-infrared light rejuvenateable persistent luminescence, *Adv. Mater.*, 2021, **33**, 2008722.

38 F. Liu, Y. Liang and Z. Pan, Detection of up-converted persistent luminescence in the near infrared emitted by the

 This journal is © the Partner Organisations 2021

Published on 25 October 2021. Downloaded by Yunnan University on 8/23/2025 5:29:18 PM.

$Zn_3Ga_2GeO_8:Cr^{3+}$, Yb^{3+}, Er^{3+} phosphor, *Phys. Rev. Lett.*, 2014, **113**, 177401.

39 Y. Chen, F. Liu, Y. Liang, X. Wang, J. Bi, X. Wang and Z. Pan, A new up-conversion charging concept for effectively charging persistent phosphors using low-energy visible-light laser diodes, *J. Mater. Chem. C*, 2018, **6**, 8003–8010.

40 Q. Gao, C. Li, Y. Liu, J. Zhang, X. Wang and F. Liu, Manipulating trap filling of persistent phosphors upon illumination by using a blue light-emitting diode, *J. Mater. Chem. C*, 2020, **8**, 6988–6992.

41 S. Yan, F. Liu, J. Zhang, X. Wang and Y. Liu, Persistent emission of narrowband ultraviolet-B light upon blue-light illumination, *Phys. Rev. Appl.*, 2020, **13**, 044051.

42 Y. Zhuang, Y. Katayama, J. Ueda and S. Tanabe, A brief review on red to near-infrared persistent luminescence in transition-metal-activated phosphors, *Opt. Mater.*, 2014, **36**, 1907–1912.

43 Z. Wang, L. Feng, J. Zhang, Z. Ci, Z. Zhang and Y. Wang, Nonequivalent substitution and charge-induced emitter-migration design of tuning spectral and duration properties of $NaCa_2GeO_4F:Mn^{2+}$ persistent luminescent phosphor, *Inorg. Chem.*, 2016, **55**, 7988–7996.

44 S. H. M. Poort, D. Cetin, A. Meijerink and G. Blasse, The luminescence of Mn^{2+}-activated $ZnGa_2O_4$, *J. Electrochem. Soc.*, 1997, **144**, 2179–2183.

45 R. Shi, L. Ning, Z. Wang, J. Chen, T. K. Sham, Y. Huang, Z. Qi, C. Li, Q. Tang and H. Liang, Zero-thermal quenching of Mn^{2+} red luminescence via efficient energy transfer from Eu^{2+} in $BaMgP_2O_7$, *Adv. Opt. Mater.*, 2019, **7**, 1901187.

46 E. Song, Y. Zhou, Y. Wei, X. Han, Z. Tao, R. Qiu, Z. Xia and Q. Zhang, A thermally stable narrow-band green-emitting phosphor $MgAl_2O_4:Mn^{2+}$ for wide color gamut backlight display application, *J. Mater. Chem. C*, 2019, **7**, 8192–8198.

47 P. Gerner, C. Fuhrer, C. Reinhard and H. U. Güdel, Near-infrared to visible photon upconversion in Mn^{2+} and Yb^{3+} containing materials, *J. Alloys Compd.*, 2004, **380**, 39–44.

48 E. Song, S. Ye, T. Liu, P. Du, R. Si, X. Jing, S. Ding, M. Peng, Q. Zhang and L. Wondraczek, Tailored near-infrared photoemission in fluoride perovskites through activator aggregation and super-exchange between divalent manganese ions, *Adv. Sci.*, 2015, **2**, 1500089.

49 W. Zhang, J. Wei, Z. Gong, P. Huang, J. Xu, R. Li, S. Yu, X. Cheng, W. Zheng and X. Chen, Unveiling the excited-state dynamics of Mn^{2+} in 0D Cs_4PbCl_6 perovskite nanocrystals, *Adv. Sci.*, 2020, **7**, 2002210.

50 M. Iwasaki, D. N. Kim, K. Tanaka, T. Murata and K. Morinaga, Red phosphorescence properties of Mn ions in $MgO–GeO_2$ compounds, *Sci. Technol. Adv. Mater.*, 2003, **4**, 137–142.

51 Y. Cong, B. Li, S. Yue, L. Zhang, W. Li and X. Wang, Enhanced red phosphorescence in $MgGeO_3:Mn^{2+}$ by addition of Yb^{3+} ions, *J. Electrochem. Soc.*, 2009, **156**, H272–H275.

52 Y. Katayama, J. Ueda and S. Tanabe, Effect of Bi_2O_3 doping on persistent luminescence of $MgGeO_3:Mn^{2+}$ phosphor, *Opt. Mater. Express*, 2014, **4**, 613–623.

53 D. J. Huntley, An explanation of the power-law decay of luminescence, *J. Phys.: Condens. Matter*, 2006, **18**, 1359–1365.

54 J. Trojan-Piegza, E. Zych, J. Holsa and J. Niittykoski, Spectroscopic properties of persistent luminescence phosphors: $Lu_2O_3:Tb^{3+},M^{2+}$ (M = Ca, Sr, Ba), *J. Phys. Chem. C*, 2009, **113**, 20493–20498.

55 F. Auzel, Upconversion and anti-stokes processes with f and d Ions in solids, *Chem. Rev.*, 2004, **104**, 139–174.

56 K. Van den Eeckhout, A. J. J. Bos, D. Poelman and P. F. Smet, Revealing trap depth distributions in persistent phosphors, *Phys. Rev. B: Condens. Matter Mater. Phys.*, 2013, **87**, 045126.

57 Y. Katayama, T. Kayumi, J. Ueda, P. Dorenbos, B. Viana and S. Tanabe, The role of Ln^{3+} (Ln = Eu, Yb) in persistent red luminescence in $MgGeO_3:Mn^{2+}$, *J. Mater. Chem. C*, 2017, **5**, 8893–8900.